Rev.Adv.Mater.Sci. 18(2008) 527-533

DEFORMATION BEHAVIOR AND FRACTOGRAPHIC FEATURES OF DUCTILE $Cu_{47}Zr_{47}Al_6$ BULK METALLIC GLASS

C. Duhamel[1,2], J. Das[1,3], S. Pauly[1], K.S. Lee[1] and J. Eckert[1,3]

[1]FG Physikalische Metallkunde, FB 11 Material- und Geowissenschaften, Technische Universität Darmstadt, Petersenstraße 23, D-64287 Darmstadt, Germany
[2]SIMAP-CNRS, Institut National Polytechnique de Grenoble, 1130, rue de la Piscine, BP 75, 38402 St Martin d'Hères, France
[3]Leibniz-Institut für Festkörper- und Werkstoffforschung Dresden, Helmholtzstraße 20, D-01069 Dresden, Germany

Received: March 29, 2008

Abstract. $Cu_{47}Zr_{47}Al_6$ bulk metallic glass rods of 2 mm diameter (Φ) are prepared by arc-melting and in-situ suction casting. The compressive deformation behavior under quasi-static conditions of the as-cast amorphous alloy exhibits a high yield strength (1600 – 1800 MPa) combined with significant plastic deformation (up to 5%). The fracture surfaces of the deformed samples consist of a mixture of vein-like patterns, river-like patterns and smooth regions. The area covered by vein-like patterns decreases when the ductility of the material increases. Protuberances, which interact strongly with the shear bands, are found at the surface of the deformed specimens.

1. INTRODUCTION

Among the recent bulk metallic glasses (BMGs) that have been designed, the Cu-base alloys have attracted extensive interest. A series of simple binary Cu-Zr [1,2] and ternary Cu-Zr-Al [3-5] BMGs and BMG composites have been reported. Moreover, it has been shown that minor addition of Y [6] or Ag [7] to the ternary system can enhance the glass forming ability. At room temperature, BMGs generally exhibit a high yield strength but a limited ductility (ε_p < 1%) [8]. However, the mechanical behavior of the Cu-Zr-base BMGs combines both high stress and enhanced ductility with plastic deformation that can reach 16% [9]. Ductility in compression has also been reported for Pt-base (ε_p = 20%) [10], Zr-base (ε_p = 4.5%) [11], Pd-base (ε_p > 170%) [12] or Ti-base (ε_p = 14.8%) [13] BMGs. Different hypotheses have been proposed to explain the enhanced ductility: (i) high Poisson's ratio [10], (ii) nanocrystallization inside the shear bands during deformation [14], (iii) liquid phase separation [15], (iv) chemical short- or medium-range order [9].

In this paper, the mechanical properties of a $Cu_{47}Zr_{47}Al_6$ BMG are reported. The deformation behavior is studied in compression under two different strain rates. SEM investigations of the fracture surfaces of the deformed samples are carried out and the observed features are correlated to the macroscopic ductility.

2. EXPERIMENTAL

The $Cu_{47}Zr_{47}Al_6$ alloy was designed by adding 6 at.% to the binary $Cu_{50}Zr_{50}$ glass forming alloy composition. The master ingots were prepared by melting the pure elements (Zr, Cu, and Al) under a Ti-gettered Ar atmosphere. 2 mm diameter cylindrical rods were obtained from the master alloys by

Corresponding author: C. Duhamel, e-mail: cecilie.duhamel@ltpcm.inpg.fr

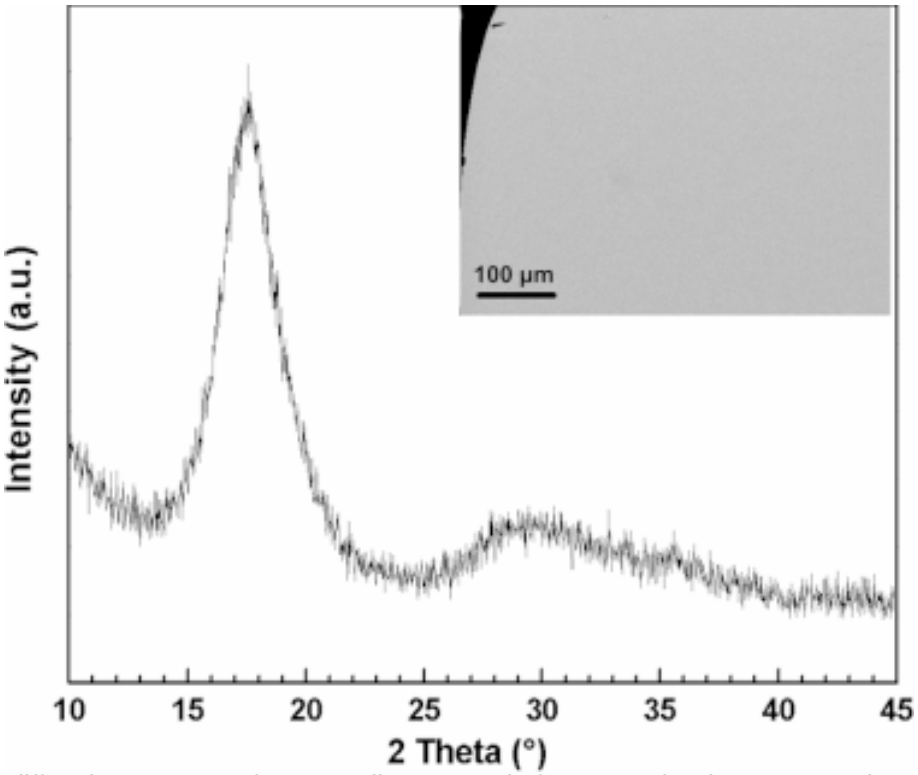

Fig. 1. X-ray diffraction patterns of a 2 mm diameter rod of $Cu_{47}Zr_{47}Al_6$. The cross-sectional microstructure of the 2 mm diameter rod, observed using back-scattered electron (BSE) mode, is shown in the inset.

using an *in-situ* suction casting facility attached to the arc-melter. The microstructure of the as-prepared rods was investigated by X-ray diffraction (XRD) in transmission geometry in a *STOE STADI P* diffractometer. Cylindrical specimens of 2 mm in diameter and 4 mm in length were prepared from the as-cast rods and tested under compression at room temperature using an Instron 5569 electromechanical testing machine at two different strain rates, $\dot{\varepsilon}=8\cdot10^{-5}$ s^{-1} and $\dot{\varepsilon}=2.5\cdot10^{-4}$ s^{-1}. The true stress σ and true strain ε are calculated from the engineering stress σ_E and strain ε_E according to the following equations:

$$\sigma = \sigma_E(1-\varepsilon_E),$$

$$\varepsilon = -\ln(1-\varepsilon_E),$$

where ε_E has been corrected from the rigidity of the testing machine estimated by comparison of the Young's modulus measured from the compression test to the one measured by ultrasonic sound velocity measurements. The fracture surfaces and the surfaces of the deformed specimens were investigated using a Zeiss DSM 962 scanning electron microscope (SEM) operated at 25 kV.

3. RESULTS AND DISCUSSION

The X-ray diffraction (XRD) pattern of the as-cast $Cu_{47}Zr_{47}Al_6$ alloy reveals two broad maxima characteristic for an amorphous structure (Fig. 1). The cross-sectional microstructure is shown in the inset of Fig. 1. No contrast is detected on the back-scattered electron (BSE) micrograph. These results are in agreement with the bulk glass formation in $(Cu_{50}Zr_{50})_{100-x}Al_x$ (x = 0 to 10) cast rods of 2-5 mm diameter reported in the literature [3]. However, the presence of nanocrystals (d < 10 nm), non detectable by XRD and SEM and observed in TEM for $Cu_{47.5}Zr_{47.5}Al_5$ alloys [9], has not been checked.

Fig. 2 shows the true stress – strain curves at room temperature, under compressive loading at two different strain rates, $\dot{\varepsilon}=2.5\cdot10^{-4}$ s^{-1} (specimens A and B) and $\dot{\varepsilon}=8\cdot10^{-5}$ s^{-1} (specimens C and D). For all the samples, a high yield strength (1603 – 1821 MPa) combined with a substantial ductility

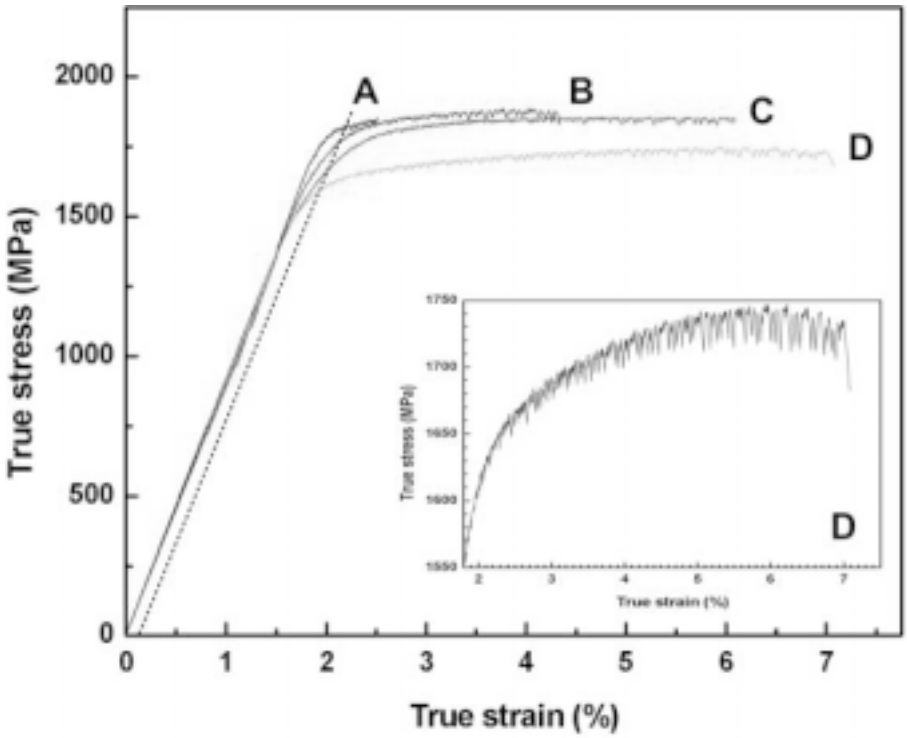

Fig. 2. True stress – true strain compression curves of the as-cast $Cu_{47}Zr_{47}Al_6$ BMG loaded at a strain rate of $2.5 \cdot 10^{-4}$ s^{-1} (A and B) and $8 \cdot 10^{-5}$ s^{-1} (C and D). The intersections between the curves an the dashed line show the yield point at 0.2% deformation. The inset is a magnified view of the curve of sample D showing the work-hardening behavior and the serrated flow occurring during deformation.

(ε_p up to 5%) is observed. The inset in Fig. 2 reveals that, after yielding, (i) a further increase of the flow stress with deformation is registered and (ii) serrated flow occurs. The magnitude of the stress drops increases with deformation from 7-10 MPa at the first stage of the plastic domain up to 25-30 MPa just before failure. The "work-hardening" behavior has already been reported for ductile $Cu_{47.5}Zr_{47.5}Al_5$ and $Ti_{45}Cu_{40}Ni_{7.5}Zr_5Sn_{2.5}$ BMG [9,13] whereas flow serrations have been observed for low strain rates [16]. Both the true stress – strain curves and the data from Table 1 suggest a strain rate dependence of the deformation behavior. With increasing the strain rate from $8 \cdot 10^{-5}$ s^{-1} to $2.5 \cdot 10^{-4}$ s^{-1}, the yield strength increases from 1603 –1676 MPa (specimens D and C respectively) to 1767 – 1821 MPa (specimens B and A respectively) whereas a significant decrease of plastic deformation from 4.10 – 5.04% (specimens C and D respectively) to 0.36 – 2.16% (specimens A and B respectively) is shown in Table 1. The effect of strain rate on the deformation behavior of bulk metallic glasses at low temperature in compression is still unclear [16,17]. However, similar effect of the strain rate on the strength was observed in compression at room temperature in a $Nd_{60}Fe_{20}Co_{10}Al_{10}$ BMG [18] and at 77K, in a $Zr_{57.4}Cu_{17.9}Ni_{13.4}Al_{10.3}Nb_1$ amorphous alloy [19]. In addition to the compression tests, the elastic properties of the $Cu_{47}Zr_{47}Al_6$ alloy were determined from ultrasonic measurements. The Young's modulus (*E*), shear modulus (μ), bulk modulus (*B*) and Poisson's ratio (ν) are 86.5 GPa, 31.2 GPa, 131 GPa and 0.39. These values are close to those reported for $Cu_{50}Zr_{50}$ and $Cu_{47.5}Zr_{47.5}Al_5$ [9] alloys.

The fracture surfaces of specimen A, deformed at $2.5 \cdot 10^{-4}$ s^{-1} and specimen C, deformed at $8 \cdot 10^{-5}$ s^{-1}, are shown on Fig. 3. All specimens failed in a shear fracture mode but significant differences in the shape of the fracture planes and the features covering them are pointed out. They strongly depend on the macroscopic ductility. The fractured specimen A, which exhibits the lowest ductility, has a conical shape (Fig. 3a). The fracture surface con-

Table 1. Room temperature compression tests results under two different strain rates for four samples of $Cu_{47}Zr_{47}Al_6$: yield strength σ_y, fracture stress σ_f and plastic deformation ε_p.

Sample	Strain rate (s^{-1})	σ_y (MPa)	σ_f (MPa)	ε_p (%)
A	2.5×10^{-4}	1821	1853	0.36
B	2.5×10^{-4}	1767	1878	2.16
C	8×10^{-5}	1676	1850	4.1
D	8×10^{-5}	1603	1734	5.04

sists in homogeneously distributed well-developed vein-like patterns (Fig. 3b), which are the classical features for the fracture surface of BMGs deformed under compressive loading [20]. They are attributed to a high temperature increase in the shear bands which is also suggested by the few molten zones and liquid droplets appearing at the fracture surface (arrows in Fig. 3b). Contrary to specimen A, a mixture of three different features is revealed on the fracture surfaces of specimens B, C, and D as exemplified in Figs. 3c and 3d for specimen C. One should notice that these three samples exhibit a plastic deformation of, at least, 2.1%. As shown in Fig. 3c, for specimen C, one half of the surface is covered by well-developed vein-like patterns (zone α). Then, an intermediary smooth region appears (zone β). On the other half of the surface, close to the edge, a mixture of well-developed river-like patterns and smooth regions is found (zone γ). It has been observed that the area covered by the vein-like patterns is reduced with an increase in the plastic deformation of the sample. This is also consistent with the features observed on specimen A, which is the less ductile sample (ε_p = 0.36%) and for which only vein-like patterns were observed. Similar mixture of vein-like patterns, river-like patterns and smooth regions has already been reported for Zr-base BMG composites and $Cu_{60}Zr_{30}Ti_{10}$ BMG deformed under compressive loading [21]. The deformed surface of specimen C shown in Fig. 3e exhibits multiple shear bands. Two main networks can be distinguished: primary shear bands (I), parallel to the fracture plane, and secondary shear bands (II), perpendicular to the first ones [9]. The spacing between the shear bands is around 150 – 200 μm. The intersection of primary and secondary shear bands leads to shear offset (black arrows in Fig. 3e). Branching of the shear bands are also observed. The branched shear bands are “wavy”, as if they were regularly “pinned” as shown by the white arrows in Fig. 3e. Such a wavy propagation of the shear bands has been reported for $Cu_{47.5}Zr_{47.5}Al_5$ [22]. Fig. 3f shows a spherical protuberance coming out from the deformed surface of sample C. Similar features are observed for samples B and D but not on sample A. Such protuberances, with a diameter of 30 – 40 μm, are either isolated and randomly distributed at the surface and/or agglomerated in one particular region (close to the fracture plane or at the opposite edge of the sample). They do not exist on the surface of the non-deformed rods and are supposed to form during deformation. However, their origin is still unclear. Profuse shear banding is observed close to these protuberances and the spacing l between shear bands is drastically decreased (λ < 5 mm).

4. SUMMARY

The deformation behavior and the fracture surface morphologies of the $Cu_{47}Zr_{47}Al_6$ BMG have been reported. The amorphous alloy exhibits high strength, enhanced ductility and work-hardening. The yield strength and plastic deformation are found to be strain rate sensitive. Examination of the fracture surfaces reveals different features, depending on the overall ductility of the deformed sample. When plastic deformation increases, the area covered by vein-like patterns decreases and new features such as river-like patterns or smooth regions appear. The surfaces of the deformed samples show that multiple shear banding occurs during deformation. Protuberances, with a 30 – 40 μm diameter and that interact strongly with shear bands, are found at the surface of the deformed amorphous samples. Such protuberances have never been reported before. Further investigations need to be carried out in order to clarify their origin.

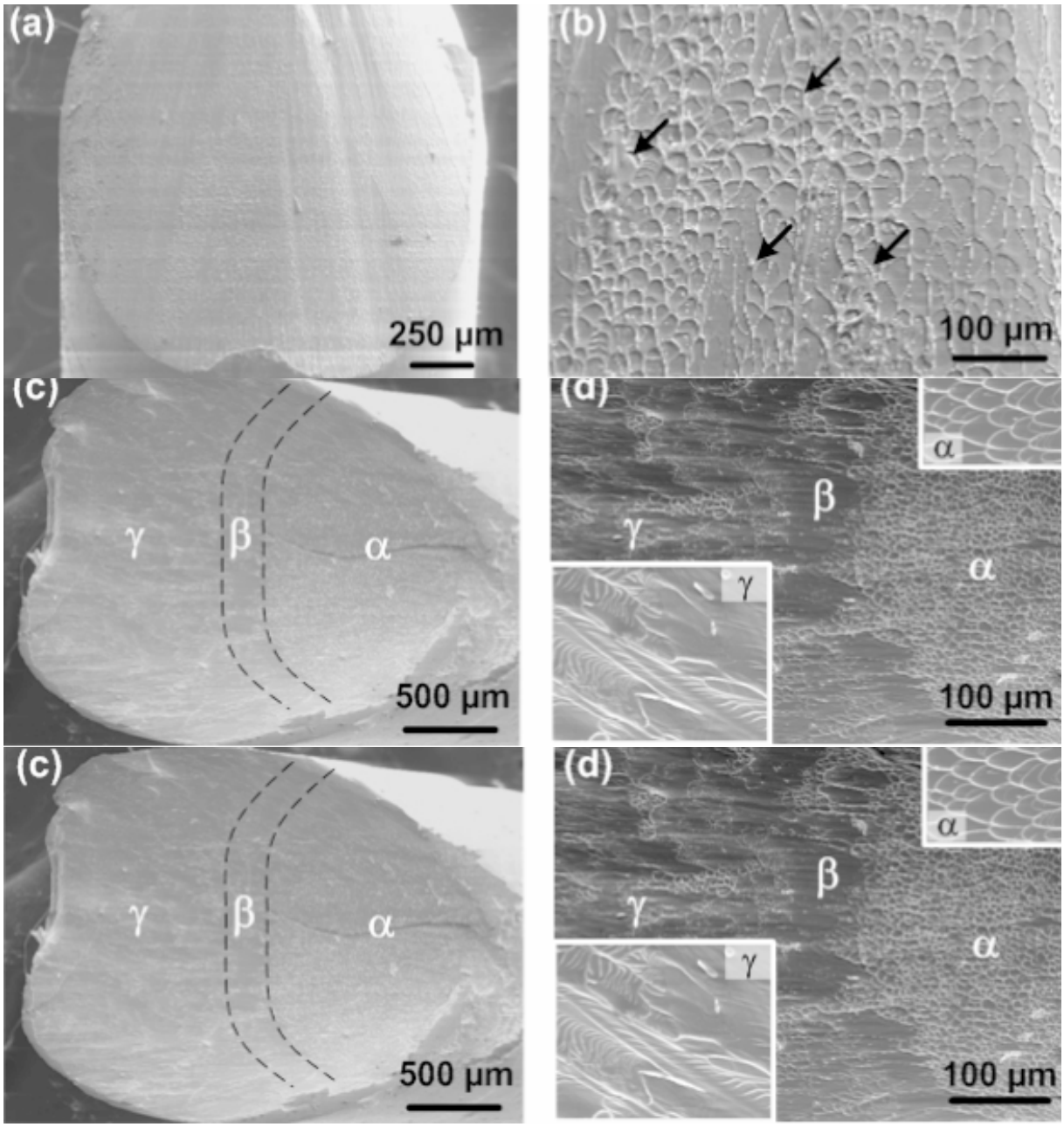

Fig. 3. Fractography of (a-b) sample A and (c-f) sample C: (a) overview of the fracture surface of the less ductile specimen (sample A); (b) enlargement of the vein-like patterns. The arrows indicate molten areas and liquid droplets; (c) overview of the fracture surface of a ductile specimen (sample C) showing three different features: vein-like patterns (α), smooth regions (β) and river-like patterns (γ), (d) enlargement of a region with the three features, (e) surface of the deformed sample C showing primary (I) and secondary (II) shear bands and shear bands with a wavy propagation (white arrows). Intersections of primary and secondary shear bands lead to shear offset (black arrows), (f) protuberance at the surface of the deformed sample C.

ACKNOWLEDGEMENTS

The authors thank M. Calin, S. Scudino, M. Stoica, S. Venkataraman, P. Yu, L.C. Zhang, W.Y. Zhang for stimulating discussions and U. Kunz, H. Lehmann, C. Wastmund for technical assistance.

REFERENCES

[1] A. Inoue, W. Zhang, T. Tsurui, A.R. Yavari and A.L. Greer // *Phil. Mag. A* **85** (2005) 221.
[2] D. Xu, B. Lohwongwatana, G. Duan, W.L. Johnson and C. Garland // *Acta Mater.* **52** (2004) 2621.
[3] P. Yu, H.Y. Bai, M.B. Tang and W.L. Wang // *J. Non-Cryst. Solids* **351** (2005) 1328.
[4] J. Das, S. Pauly, C. Duhamel, B.C. Wei and J. Eckert // *J. Mater. Res.*, accepted for publication.
[5] Y.F. Sun, B.C. Wei, Y.R. Wang, W.H. Li, T.L. Cheung and C.H. Shek // *Appl. Phys. Lett.* **87** (2005) 051905.
[6] D. Xu, G. Duan and W.L. Johnson // *Phys. Rev. Lett.* **92** (2004) 245504.
[7] D.S. Sung, O.J. Kwon, E. Fleury, K.B. Kim, J.C. Lee, D.H. Kim and Y.C. Kim // *Met. Mater. Inter.* **10** (2004) 575.
[8] H.A. Bruck, T. Christman, A.J. Rosakis and W.L. Johnson // *Scripta Metall. Mater.* **30** (1994) 429.
[9] J. Das, M.B. Tang, K.B. Kim, R. Theissmann, F. Baier, W.H. Wang and J. Eckert // *Phys. Rev. Lett.* **94** (2005) 205501.
[10] J. Schroers and W.L. Johnson // *Phys. Rev. Lett.* **93** (2004) 255506.
[11] L.Q. Xing, Y. Li, K.T. Ramesh, J. Li and T.C. Hufnagel // *Phys. Rev. B* **64** (2001) 180201.
[12] K.F. Yao, F. Ruan, Y.Q. Yang and N. Chen // *Appl. Phys. Lett.* **88** (2006) 122106.
[13] K.B. Kim, J. Das, S. Venkataraman, S. Yi and J. Eckert // *Appl. Phys. Lett.* **89** (2006) 071908.
[14] J. Saida, A.D.H. Setyawan, H. Kato and A. Inoue // *Appl. Phys. Lett.* **87** (2005) 151907.
[15] J.C. Oh, T. Ohkubo, Y.C. Kim, E. Fleury and K. Hono // *Scripta Mater.* **53** (2005) 165.
[16] T. Mukai, T.G. Nieh, Y. Kawamura, A. Inoue and K. Higashi // *Intermetallics* **10** (2002) 1071.
[17] H.A. Bruck, A.J. Rosakis and W.L. Johnson // *J. Mater. Res.* **11** (1996) 503.
[18] L.F. Liu, L.H. Dai, Y.L. Bai, B.C. Wei and G.S. Yu // *Intermetallics* **13** (2005) 827.
[19] H. Li, C. Fan, K. Tao, H. Choo and P.K. Liaw // *Adv. Mater.* **18** (2006) 752.
[20] Z.F. Zhang, J. Eckert and L. Schultz // *Acta Mater.* **51** (2003) 1167.
[21] M. Kusy, U. Kühn, A. Concustell, A. Gebert, J. Das, J. Eckert, L. Schultz and M.D. Baro // *Intermetallics* **14** (2006) 982.
[22] K.B. Kim, J. Das, F. Baier, M.B. Tang, W.H. Wang and J. Eckert // *Appl. Phys. Lett.* **88** (2006) 051911.